Computational and Structural Biotechnology Journal 19 (2021) 4669–4675

COMPUTATIONAL AND STRUCTURAL BIOTECHNOLOGY JOURNAL

journal homepage: www.elsevier.com/locate/csbj

Non-conventional interactions of N3 inhibitor with the main protease of SARS-CoV and SARS-CoV-2

Ponciano García-Gutiérrez [a], Rafael A. Zubillaga [a], Ilich A. Ibarra [b], Ana Martínez [b], Rubicelia Vargas [a,*], Jorge Garza [a,*]

[a] Departamento de Química, División de Ciencias Básicas e Ingeniería, Universidad Autónoma Metropolitana-Iztapalapa, San Rafael Atlixco 186, Col. Vicentina, Iztapalapa 09340, Ciudad de México, Mexico
[b] Instituto de Investigaciones en Materiales, Universidad Nacional Autónoma de México, Circuito Exterior S. N., Ciudad Universitaria, Coyoacán 04510, Ciudad de México, Mexico

ARTICLE INFO

Article history:
Received 30 April 2021
Received in revised form 9 August 2021
Accepted 9 August 2021
Available online 12 August 2021

Keywords:
COVID-19
Non-covalent bonds
Hydrogen bonds
QTAIM
DFT
N3 complexes

ABSTRACT

The extensive spread of COVID-19 in every continent shows that SARS-CoV-2 virus has a higher transmission rate than SARS-CoV virus which emerged in 2002. This results in a global pandemic that is difficult to control. In this investigation, we analyze the interaction of N3 inhibitor and the main protease of SARS-CoV and SARS-CoV-2 by quantum chemistry calculations. Non-covalent interactions involved in these systems were studied using a model of 469 atoms. Density Functional Theory and Quantum Theory of Atoms in Molecules calculations lead us to the conclusion that non-conventional hydrogen bonds are important to describe attractive interactions in these complexes. The energy of these non-conventional hydrogen bonds represents more than a half of the estimated interaction energy for non-covalent contacts. This means that hydrogen bonds are crucial to correctly describe the bonds between inhibitors and the main proteases. These results could be useful for the design of new drugs, since non-covalent interactions are related to possible mechanisms of action of molecules used against these viruses.

1. Introduction

Everyone knows and is suffering the consequences of the Global Health Crisis from COVID-19 outbreak, and we all recognize that our society faces the greatest challenge since World War II. There are reports [1] that almost prophetically warned us about this situation in 2015, but we do not imagine the magnitude of the problem we should face. There is still a controversy about the origin of the virus that causes COVID-19, but regardless of whether SARS-CoV-2 comes from bats or some other source, this pandemic has claimed human lives around the world. The extensive spread of COVID-19 in every continent shows that SARS-CoV-2 virus has a higher transmission rate than SARS-CoV virus which emerged in 2002 [2]. This results in a global pandemic that is difficult to control.

SARS-CoV-2 is a coronavirus that belongs to *Coronaviridae* [3] family. These are enveloped viruses with a positive-strand RNA genome. These coronaviruses mainly contain four structural proteins: spike protein, envelope protein, membrane protein, and nucleocapsid protein [4]. Spike proteins are relevant during the virus infection since they promote host attachment with virus–cell membrane fusion.

SARS-CoV-2 is a new coronavirus but there are others that can be used as a model to take advantage of the knowledge and experience. From the comparison with different proteases of other coronaviruses, it has been demonstrated that the main protease is a conserved drug target [3]. It was previously reported [5] that all main proteases of CoV viruses have a highly conserved substrate-recognition pocket. The X-ray crystal structure of the main protease of SARS-CoV-2 was published in February 2020 [6] and it was demonstrated that it has a dimer-like structure that is similar (96%) of that of SARS-CoV [7,8].

Several compounds have been investigated to find antiviral drugs against human COVID-19 infection [6] but an effective and unquestionable antiviral strategy is not yet available. One possible goal is to find an inhibitor of the main proteasa of SARS-CoV-2 (named here as SARS-CoV-2-Mpro). This idea comes from the results of SARS-CoV that is a well-studied coronavirus. In 2016 it was reported the crystal structure of a synthetic peptidomimetic inhibitor (N3, see Fig. 1). This molecule forms a complex with the main proteasa of SARS-CoV (named here as SARS-CoV-Mpro) [3]

* Corresponding authors.
E-mail addresses: ruvf@xanum.uam.mx (R. Vargas), jgo@xanum.uam.mx (J. Garza).

https://doi.org/10.1016/j.csbj.2021.08.015

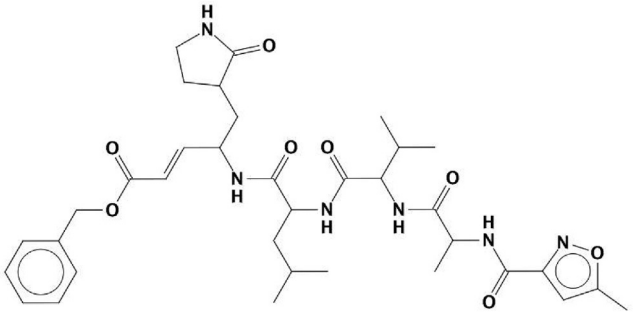

Fig. 1. Molecular structure of N3 inhibitor.

and this helps controlling the infections. The similarity of SARS-CoV-2 with SARS-CoV virus is certainly important for the design of new inhibitors. This allows us to think that it is possible to develop inhibitors against SARS-CoV-2-Mpro using the information that we already have for SARS-CoV-Mpro.

The crystal structure of N3 interacting with SARS-CoV-2-Mpro was already published [6]. Authors report specific interactions of N3 with SARS-CoV-2-Mpro and they compared with the result of SARS-CoV-Mpro. They conclude that bonds of N3 with the main proteases are similar in both cases and therefore, the action mechanisms should be alike. However, these are X-ray structural data and with these results it is not possible to fully characterize molecular bonds.

Without a doubt, it is important to analyse all inhibitor-protein interactions. The number of reports with classical molecular dynamics techniques is increasing since it is possible to study these biological systems [9–13]. Details of such interactions can be obtained by using quantum chemistry calculations [14,15]. Nevertheless the size of these systems is an important restriction for these methods. Fragment molecular orbital-based interaction analysis has been used to estimate interaction energies [16,17,13,18–20]. In spite of all these investigations, there are no characterizations of non-covalent interactions of SARS-CoV-Mpro and SARS-CoV-2-Mpro with N3. For this reason, in this investigation we determine and compare all interactions of N3 with these two main proteases. Hydrogen bonds are characterized in this work using Quantum Theory of Atoms in Molecules (QTAIM) [21]. From this theoretical analysis, we determine the differences between complexes of N3 interacting with SARS-CoV-Mpro and SARS-CoV-2-Mpro. These results could contribute to the development of effective drugs against COVID-19.

2. Methods

Crystals structures of SARS-CoV-Mpro and SAR-CoV-2-Mpro interacting with N3 indicate that there is a C-S covalent bond of CYS144 of the main protease and PJE of N3. To identify and quantify intermolecular interactions between N3 and SARS-CoV-Mpro (PDB ID2AMQ) or SARS-CoV-2-Mpro (PDB ID6LU7), some reduced molecular systems were constructed from X-ray crystallographic structures as follows: a) water molecules were removed from structures; b) hydrogen atoms were added; c) ionic residues were protonated or deprotonated according to Protonate-3D application assuming a pH equal to 7.0; and d) the reduced systems included those protease residues with at least one atom at maximum 4.0 Å from any atom of N3, all residues outside this cut-off value were eliminated, and the resulting peptide fragments were capped at the N- and C- termini by methylation. Both models contain 469 atoms, 97 from the inhibitor and 372 atoms related to the cavity of the corresponding protease.

In order to obtain optimized structure conformations of SARS-CoV-Mpro and SARS-CoV-2-Mpro complexed with N3, we performed molecular dynamics (MD) simulations for both complexes. The systems were centered in a cubic box and solvated with 39,103 (SARS-CoV-Mpro-N3) and 33,420 water molecules (SARS-CoV-2-Mpro-N3). Both systems were neutralized with two Na^+ ions. The force field was the hybrid AMBER10–EHT, that is parameterized for proteins and small molecules [22,23]. For all simulations, temperature was 310 K and the pH was 7.0. NVT simulations were performed using the Nosé-Poincaré-Andersen equations of motion [24] and the production MD was run for 10 ns with a time step of 0.002 ps. The final conformations were used to build other two reduced systems. We calculated again the intermolecular interactions between N3 and SARS-CoV-Mpro or SARS-CoV-2-Mpro with these two models, applying the previously described protocol. These four reduced systems are included in the electronic supporting information (ESI). Molecular modeling and MD simulations were performed with Molecular Operating Environment software [25].

The two reduced systems corresponding to crystallographic conformations of the protease-inhibitor complexes are shown in Fig. 2. The electronic structure of all systems was obtained in the gas phase at PBE0-D3/6-311G(d,p) [26,27] level of theory with the Terachem code [28]. All geometries were partially optimized since only the position of all hydrogen atoms was optimized. Molecular Electrostatic Potential [29], Non-Covalent Interaction index (NCI) [30] and QTAIM scalar fields were obtained by the graphics processing units for atoms and molecules (GPUAM) project [31,32] developed in our group.

3. Results and discussion

N3 inhibitor is a molecule with different rotamers, as can be seen in Fig. 3 were three possible structures are reported. Rotamer (**I**) corresponds to the structure observed in the crystallographic structure of the complex formed with SARS-CoV-2-Mpro. This molecule was obtained from the crystal structure optimizing only the position of the hydrogen atoms. The other two geometries of Fig. 3 (**II** and **III**) were fully optimized. The details of these three structures are reported in the ESI. The structure of the rotamers **II** and **III** is not similar between them but their energy difference is small (2.4 kcal/mol) and therefore both structures should be present under experimental conditions. One important characteristic of this molecule is the number of lone pairs given by oxygen and nitrogen atoms. This generates a particular feature of the Molecular Electrostatic Potential (MEP). MEP is reported on the right side of Fig. 3 for rotamer (III) as an example, since it is similar for the three structures. MEP indicates that this molecule has several positive and negative regions that induce possible contacts with the main protease of coronaviruses. These interactions should be driven by electrostatic effects.

Fig. 4 reports isosurfaces of the electron density and the NCI for the systems under study in X-ray. In this figure, NCI is represented with an isosurface colored mainly in green, which indicates weak interactions (van der Waals and hydrogen bonds) between N3 and the main protease, and also intramolecular interactions. These isosurfaces form boundary between the electron densities delivered by our main protease models and the N3 molecule. NCI reveals weak non-covalent interactions for both molecular systems, and without a doubt there are many non-covalent interactions between N3 and the main proteases. From results of NCI, all possible critical points of the electron density were investigated in order to characterize all the interactions through the QTAIM approach for X-ray and MD structures. We count all the interactions between N3 and the main proteasa models looking for Bond

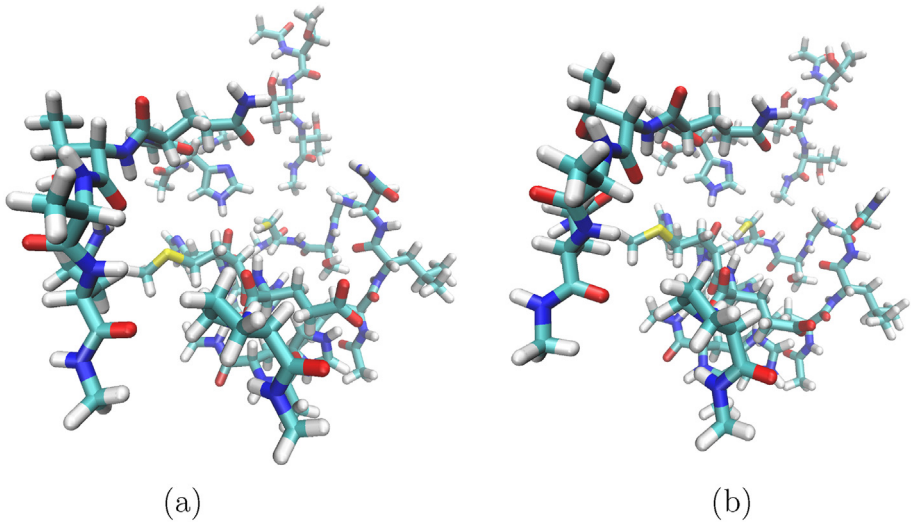

Fig. 2. Cavities of the main proteasa of (a) SARS-CoV-Mpro and (b) SARS-CoV-2-Mpro.

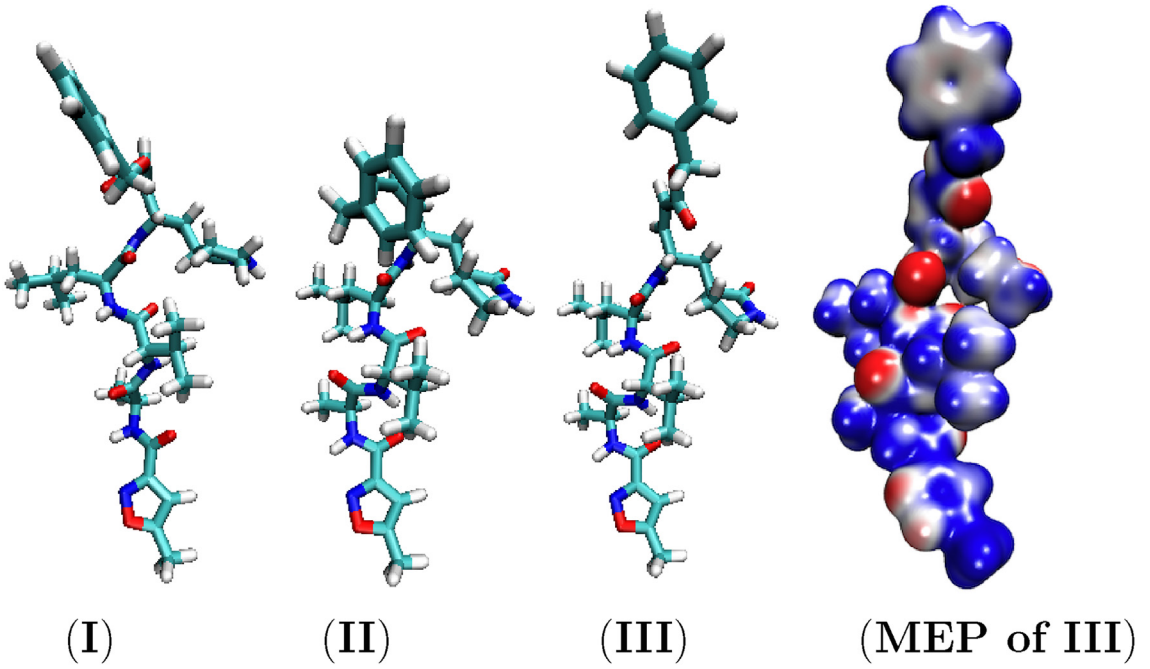

Fig. 3. Three rotamers of the N3 inhibitor. The Molecular Electrostatic Potential (MEP) of the rotamer (**III**) is depicted on the right side as an example. Blue regions indicate positive values and red zones indicate negative values.

Critical Points (BCP, defined within QTAIM). With BCP it is possible to obtain the corresponding bond paths and therefore to establish the atoms involved in each interaction. With this information we determine the molecular graph of each modeled complex. As example, in Figs. 4**b** and 4**d** we present the bond paths (in pink color) for both complexes considered in this article related to X-ray structures. From here, we characterize each bond between N3 interacting with SARS-CoV-2-Mpro and SARS-CoV-Mpro. Table 1 reports a summary of the QTAIM analysis performed to obtain the hydrogen bonds related to the interaction between N3 and the main proteasa of SARS-CoV and SARS-CoV-2.

The QTAIM analysis indicates that there is an impressive number of hydrogen bonds in both complexes (see results of Table 1). In this table we include the following parameters that characterize the hydrogen bonds: i) distance between hydrogen atom (H) and the acceptor atom (A); ii) distance between acceptor atoms (A) and donor atom (D); iii) angle $\measuredangle$A···H-D defined by the three atoms involved in the hydrogen bond; iv) electron density evaluated at each BCP; ρ(BCP), corresponding to the hydrogen bond. For each parameter we are reporting the smallest value (top), the average (middle and bold font) and the highest value (bottom). More specific information of hydrogen bonds for all systems is given in ESI. It is important to mention that we have considered only those contacts that exhibit $\rho(\text{BCP}) \geq 0.001$ au. From the data reported in this table, it is evident that N–H···O, C–H···O, C–H···C, and C–H···N hydrogen bonds are important in these complexes. N–H···O hydrogen bonds exhibit geometrical parameters which induce appropriately this interaction, with relatively small A···H and A···D distances, and large $\measuredangle$A···H-D angle. It is worth to mention that this hydrogen bond seems stronger in the complex of N3

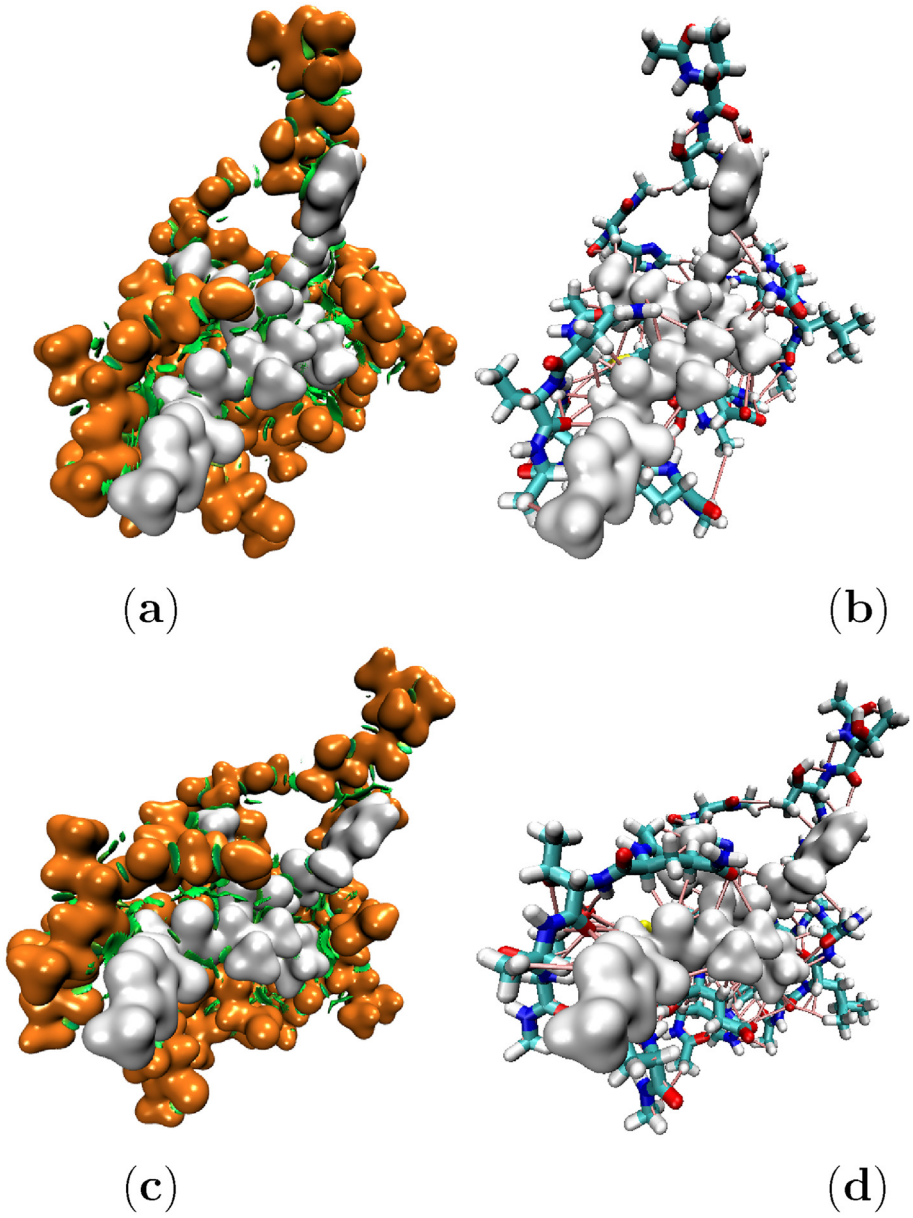

Fig. 4. Isosurfaces of the electron density (orange for protase and white for inhibitor) and non-colvalent interaction index (green) for (**a**) N3 interacting with SARS-CoV-Mpro and (**c**) N3 interacting with SARS-CoV-2-Mpro. Inter- and intra-molecular contacts depicted through bond paths (pinks) provided by the QTAIM for (**b**) N3 interacting with SARS-CoV-Mpro and (**d**) N3 interacting with SARS-CoV-2-Mpro systems.

with SARS-CoV-2-Mpro than that observed with SARS-CoV-Mpro (see values presented in Table 1). It is also important to mention that there are eight of these interactions in the complex of N3 with SARS-CoV-2-Mpro and seven in the complex of N3 with SARS-CoV-Mpro for X-ray structures. The number of these contacts is increased in the structures obtained from MD, indicating that these hydrogen bonds are favored by using this methodology.

The C–H···O interation has been recognized as a weak hydrogen bond, with high relevance to stabilize some systems [33]. In all complexes considered in this article, it is clear the importance of these interactions since for X-ray structures there are 25 interactions with SARS-CoV-Mpro and 27 with SARS-CoV-2-Mpro. The number of these contacts is reduced in the structures predicted by MD (20 and 18). Thus, this hydrogen bond is less favored in MD. We cannot overlook the role of the -H···H- contact (dihydrogen bond [34]) since it appears several times in each complex; in fact, from Table 1 we observe a smaller contact distance than that found for C–H···O interactions. C–H···N, C–H···C, C–H···S, N–H···N, and N–H···C, present a small number of contacts although the contribution of all of them cannot be neglected; also, we observed that N–H···N is present in X-ray structures and does not in MD, instead a N–H···C appears.

For non-covalent interactions we use the Espinosa-Molins-Lecomte (EML) approach [35] to estimate the energy involved in each hydrogen bond. In this approach, the kinetic energy density and the potential energy density at the bond critical points in hydrogen bonds are reduced from topological analyses of experimental electron distribution extracted from X-ray diffraction experiments. This approximation is quite useful to compare binding energies between two similar systems, but it cannot be used to estimate thermodynamics binding properties. From this analysis we found that the complex of N3 with SARS-CoV-Mpro exhibits the highest interaction energy related to hydrogen bonds. We do arbitrarily assign 100.0 to this interaction energy. Within this scale, the

Table 1
Hydrogen bonds obtained for N3 interacting with SARS-CoV-Mpro and N3 interacting with SARS-CoV-2-Mpro models. d(A···H) represents the distance between a hydrogen atom (H) and the acceptor (A), d(A···D) the distance between acceptor and donor (D), and ∢A···H-D the angle involved in the hydrogen bond. The electron density evaluated at a critical point corresponding to a hydrogen bond is represented by ρ(BCP).

Hydrogen bond	N3 interacting with SARS-CoV-Mpro					N3 interacting with SARS-CoV-2-Mpro				
	#	d(A–H)	d(A–D)	∢A–H-D	ρ(BCP)	#	d(A–H)	d(A–D)	∢A–H-D	ρ(BCP)
					X-ray structures					
		1.615	2.639	104.5	0.004		1.795	2.803	149.8	0.004
N–H···O	7	**2.162**	**3.026**	**150.7**	**0.022**	8	**2.073**	**3.054**	**163.1**	**0.023**
		2.763	3.529	173.6	0.054		2.815	3.724	172.7	0.034
		1.516	2.508	113.1	0.001		2.124	2.622	104.3	0.001
C–H···O	25	**2.563**	**3.389**	**134.8**	**0.013**	27	**2.740**	**3.520**	**131.0**	**0.007**
		3.509	4.346	154.3	0.069		3.339	4.096	168.2	0.024
		2.402	2.868	103.4	0.003		–	–	–	–
C–H···C	6	**2.671**	**3.490**	**136.3**	**0.010**	0	–	–	–	–
		3.158	4.215	162.3	0.016		–	–	–	–
		2.407	3.365	108.0	0.002		2.533	3.310	117.8	0.002
C–H···N	5	**3.192**	**3.965**	**133.0**	**0.004**	8	**2.860**	**3.701**	**134.9**	**0.007**
		3.461	4.396	168.0	0.014		3.591	4.420	153.2	0.011
		3.576	4.118	112.4	0.002					
C–H···S	2	**3.647**	**4.416**	**132.5**	**0.002**	1	**2.977**	**3.949**	**148.6**	**0.007**
		3.718	4.714	152.5	0.003					
N–H···N	1	**3.211**	**3.976**	**133.7**	**0.002**	0	–	–	–	–
		1.918	–	–	0.003		1.554	–	–	0.002
H···H	16	**2.265**	–	–	**0.007**	15	**2.249**	–	–	**0.007**
		2.755	-	–	0.014		2.993	–	–	0.029
					Molecular dynamics structures					
		1.820	2.771	120.3	0.003		1.846	2.907	117.1	0.007
N–H···O	10	**2.169**	**3.068**	**153.1**	**0.020**	9	**2.147**	**3.074**	**157.0**	**0.018**
		3.024	3.646	176.2	0.031		2.650	3.338	170.4	0.029
		2.297	3.076	105.9	0.002		2.389	3.112	110.9	0.001
C–H···O	20	**2.735**	**3.530**	**132.5**	**0.007**	18	**2.835**	**3.665**	**134.6**	**0.006**
		3.315	4.027	172.8	0.014		3.850	4.764	166.0	0.011
		2.742	3.664	142.0	0.003		2.116	2.939	131.7	0.005
C–H···C	4	**3.022**	**4.002**	**150.2**	**0.004**	4	**2.859**	**3.825**	**148.1**	**0.033**
		3.112	4.334	159.2	0.006		3.530	4.580	158.1	0.091
		2.496	3.336	116.6	0.002		2.740	3.480	132.9	0.002
C–H···N	5	**2.940**	**3.811**	**139.8**	**0.006**	3	**2.862**	**3.786**	**143.1**	**0.006**
		3.398	4.338	165.7	0.012		3.303	4.129	153.0	0.010
		2.836	3.498	119.0	0.003					
C–H···S	3	**3.128**	**3.982**	**137.4**	**0.006**	1	**2.944**	**4.001**	**162.8**	**0.007**
		3.479	4.473	151.9	0.009					
N–H···C	0	–	–	–	–	1	**2.981**	**3.712**	**130.3**	**0.004**
		2.011	–	–	0.001		1.970	–	–	0.002
H···H	10	**2.468**	–	–	**0.005**	11	**2.326**	–	–	**0.007**
		3.077	–	–	0.011		2.708	–	–	0.011

complex of N3 with SARS-CoV-2-Mpro exhibits a relative interaction energy of 74.6 for X-ray structures, and it is 88.6 for MD structures. Thus, the energetic contribution of these interactions is higher for the complex of N3 with SARS-CoV-Mpro than that observed with SARS-CoV-2-Mpro.

Based on this energy analysis, the contribution (in percent) of each hydrogen bond is reported in Table 2. The N–H···O hydrogen bond has an important contribution to the stabilization energy with the EML approximation. From MD structures, this hydrogen bond represents about half of the total interaction energy. Even

Table 2
Energy contribution, in percent, of each hydrogen bond type found in N3 interaction with SARS-CoV-Mpro and N3 interacting with SARS-CoV-2-Mpro complexes. "Others" represent C–H···N, C–H···S, N–H···N, and N–H···C hydrogen bonds.

Modeled complex	Hydrogen bond type			
	N–H···O	C–H···O	-H···H-	Others
		X-ray structures		
N3 with SARS-CoV-Mpro	25.8	53.3	11.3	9.6
N3 with SARS-CoV-2-Mpro	37.4	34.1	19.9	8.6
		MD structures		
N3 with SARS-CoV-Mpro	52.2	27.4	8.9	11.5
N3 with SARS-CoV-2-Mpro	45.5	24.7	14.5	15.3

in these structures, the contribution of non-conventional hydrogen bonds is significant. From this table, we observe that each contribution depends on the analyzed structure. The results with MD indicate that there is an increment of the N–H···O hydrogen bond contribution, but there is a decrease in the energy contribution of others hydrogen bonds, in particular the C–H···O contact. The possible explanation for these results with MD is that, within this approach, the packing of the structure relaxes and/or MD underestimates the interaction energy of non-conventional hydrogen bonds. We conclude that the fitted parameters involved in the force fields should be revised for non-conventional hydrogen bonds.

The positions of hydrogen atoms predicted by our computational methodology is important since we comprehensively described all the hydrogen bonds involved in the inhibitor-main protease interaction. Other methodologies to describe inhibitor-protease interactions are based on molecular mechanics that use parametrizations for the description of the hydrogen bonds. We are stressing that for the complexes of N3 with SARS-CoV-Mpro and SARS-CoV-2-Mpro, there are many non-conventional hydrogen bonds that must be considered in such parametrization. In fact, for the analyzed structures unconventional hydrogen bonds contribute as much or more than conventional N–H···O hydrogen bonds, as can be seen in Table 2.

From these analysis we obtained a full characterization of non-covalent interactions of both complexes, and we can determine the small differences between them. These differences, despite being small, affect the way that N3 binds to the main protease and therefore could change its ability to inhibit the virus.

4. Conclusions

Hydrogen bonds between N3 inhibitor and SARS-CoV-Mpro or SARS-CoV-2-Mpro are characterized through QTAIM. From this analysis we found that non-conventional hydrogen bonds are important to describe attractive interactions in these complexes. These interactions are not usually considered by classical molecular dynamics techniques. Thus, the results provided by this article could be considered to fit force fields in order to have a better description of this kind of systems.

N3 can specifically inhibit main proteasas from multiple coronaviruses, including SARS-CoV, and has displayed potent antiviral activity against infectious. To elucidate the inhibitory mechanism of N3, it is important to characterized all the interactions as we report in this investigation. The small differences that we found between SARS-CoV and SARS-CoV-2 main proteasas could modify the activity of N3. These differences, despite being small, affect the way that N3 binds to the main protease and therefore could change its ability to inhibit the virus.

Main proteasas present a substrate-recognition pocket that is highly conserved among all coronaviruses. This pocket could serve as a drug target for the design of broad-spectrum inhibitors. In this investigation, the model that we used for the main proteasas of SARS-CoV and SARS-CoV-2 represents this pocket. Therefore, the non-covalent interactions with N3 that we report here characterized the systems and could serve for the design of new inhibitors.

Declaration of Competing Interest

The authors declare that they have no known competing financial interests or personal relationships that could have appeared to influence the work reported in this paper.

Acknowledgements

This work was supported by CONACYT, México, through the project FC- 2016/2412. The authors thank the facilities provided by the Laboratorio de Supercómputo y Visualización en Paralelo at the Universidad Autónoma Metropolitana -Iztapalapa. AM thanks to LANCAD-UNAM-DGTIC-141.

Appendix A. Supplementary data

Supplementary data associated with this article can be found, in the online version, athttps://doi.org/10.1016/j.csbj.2021.08.015.

References

[1] Menachery VD, Yount Jr BL, Debbink K, Agnihothram S, Gralinski LE, Plante JA, Graham RL, Scobey T, Ge X-Y, Donaldson EF, Randell SH, Lanzavecchia A, Marasco WA, Shi Z-L, Baric RS. A SARS-like cluster of circulating bat coronaviruses shows potential for human emergence. Nat. Med. 2015;21:1508–13.
[2] South AM, Tomlinson L, Edmonston D, Hiremath S, Sparks MA. Controversies of renin-angiotensin system inhibition during the COVID-19 pandemic. Nat. Rev. Nephrol. 2020. https://doi.org/10.1038/s41581-020-0279-4.
[3] Wang F, Chen C, Tan W, Yang K, Yang H. Structure of Main Protease from Human Coronavirus NL63: Insights for Wide Spectrum Anti-Coronavirus Drug Design. Sci. Rep. 2016;6:22677.
[4] Bosch B, van der Zee R, de Haan C, Rottier P. The coronavirus spike protein is a class I virus fusion protein: Structural and functional characterization of the fusion core complex. J. Virol. 2003;77:8801–11.
[5] Yang H, Xie W, Xue X, Yang K, Ma J, Liang W, Zhao Q, Zhou Z, Pei D, Ziebuhr J, Hilgenfeld R, Yuen K, Wong L, Gao G, Chen S, Chen Z, Ma D, Bartlam M, Rao Z. Design of wide-spectrum inhibitors targeting coronavirus main proteases. PLoS. Biol. 2005;3:1742–52.
[6] Jin Z, Du X, Xu Y, Deng Y, Liu M, Zhao Y, Zhang B, Li X, Zhang L, Peng C, Duan Y, Yu J, Wang L, Yang K, Liu F, Jiang R, Yang X, You T, Liu X, Yang X, Bai F, Liu H, Liu X, Guddat LW, Xu W, Xiao G, Qin C, Shi Z, Jiang H, Rao Z, Yang H. Structure of Mpro from SARS-CoV-2 and discovery of its inhibitors. Nature 2020. https://doi.org/10.1038/s41586-020-2223-y.
[7] Anand K, Ziebuhr J, Wadhwani P, Mesters J, Hilgenfeld R. Coronavirus main proteinase (3CL(pro)) structure: Basis for design of anti-SARS drugs. Science 2003;300(5626):1763–7.
[8] Yang H, Yang M, Ding Y, Liu Y, Lou Z, Zhou Z, Sun L, Mo L, Ye S, Pang H, Gao G, Anand K, Bartlam M, Hilgenfeld R, Rao Z. The crystal structures of severe acute respiratory syndrome virus main protease and its complex with an inhibitor. Proc. Natl. Acad. Sci. U.S.A. 2003;100:13190–5.
[9] Cetin A. In silico studies on stilbenolignan analogues as SARS-CoV-2 Mpro inhibitors. Chem. Phys. Lett. 2021;771:138563.
[10] Scior T, Abdallah HH, Mustafa SFZ, Guevara-García JA, Rehder D. Are vanadium complexes druggable against the main protease Mpro of SARS-CoV-2? – A computational approach. Inorg. Chim. Acta 2021;519:120287.
[11] Awoonor-Williams E, Abu-Saleh AA-AA. Covalent and non-covalent binding free energy calculations for peptidomimetic inhibitors of SARS-CoV-2 main protease. Phys. Chem. Chem. Phys. 2021;23:6746–57.
[12] Chhetri A, Chettri S, Rai P, Mishra DK, Sinha B, Brahman D. Synthesis, characterization and computational study on potential inhibitory action of novel azo imidazole derivatives against COVID-19 main protease (Mpro: 6LU7). J. Mol. Struct. 2021;1225:129230.
[13] Hatada R, Okuwaki K, Akisawa K, Mochizuki Y, Handa Y, Fukuzawa K, Komeiji Y, Okiyama Y, Tanaka S. Appl. Phys. Express 2021;14:027003.
[14] Yañez O, Osorio MI, Uriarte E, Areche C, Tiznado W, Pérez-Donoso JM, García-Beltrán O, González-Nilo F. In silico study of coumarins and quinolines derivatives as potent inhibitors of SARS-CoV-2 main protease. Front. Chem. 2021;8:1273.
[15] O. Yañez, O.M.I., C. Areche, A. Vasquez-Espinal, J. Bravo, A. Sandoval-Aldana, J. M. Pérez-Donoso, F. González-Nilo, M.J. Matos, E. Osorio, O. García-Beltrán, W. Tiznado, Theobroma cacao l. compounds: Theoretical study and molecular modeling as inhibitors of main SARS-CoV-2 protease, Biomed. Pharmacother. 140 (2021) 111764..
[16] Hatada R, Okuwaki K, Mochizuki Y, Fukuzawa K, Komeiji Y, Okiyama Y, Tanaka S. Fragment Molecular Orbital Based Interaction Analyses on COVID-19 Main Protease - Inhibitor N3 Complex (PDB ID:6LU7. J. Chem. Inf. Model. 2020;60:3593–602.
[17] Takaya D, Watanabe C, Nagase S, Kamisaka K, Okiyama Y, Moriwaki H, Yuki H, Sato T, Kurita N, Yagi Y, Takagi T, Kawashita N, Takaba K, Ozawa T, Takimoto-Kamimura M, Tanaka S, Fukuzawa K, Honma T. FMODB: The world's first database of quantum mechanical calculations for biomacromolecules based on the fragment molecular orbital method. J. Chem. Inf. Model. 2021;61:777–94.
[18] Tam NM, Nam PC, Quang DT, Tung NT, Vu VV, Ngo ST. Binding of inhibitors to the monomeric and dimeric SARS-CoV-2 Mpro. RSC Adv. 2021;11:2926–34.

[19] Watanabe C, Okiyama Y, Tanaka S, Fukuzawa K, Honma T. Molecular recognition of SARS-CoV-2 spike glycoprotein: quantum chemical hot spot and epitope analyses. Chem. Sci. 2021;12:4722–39.
[20] Kato K, Honma T, Fukuzawa K. Intermolecular interaction among Remdesivir, RNA and RNA-dependent RNA polymerase of SARS-CoV-2 analyzed by fragment molecular orbital calculation. J. Mol. Graph. Model. 2020;100:107695.
[21] Bader RFW. Atoms in molecules: A quantum theory, International series of monographs on chemistry. Clarendon Press; 1990.
[22] Case DA, Cheatham T, Darden T, Gohlke H, Luo R, Merz Jr KM, Onufriev A, Simmerling C, Wang B, Woods R. The Amber biomolecular simulation programs. J. Comput. Chem. 2005;26:1668–88.
[23] Gerber P, Müller K. Mab, a generally applicable molecular force field for structure modelling in medicinal chemistry. J. Computer-Aided Mol. Des. 1995;9:251–68.
[24] Sturgeon JB, Laird BB. Symplectic algorithm for constant pressure molecular dynamics using a nosé–poincaré thermostat 2000;112:3474–82.
[25] Chemical Computing Group Inc, Montreal, QC, Canada, Molecular Operating Environment 2016.08 (2016)..
[26] Adamo C, Barone V. Toward reliable density functional methods without adjustable parameters: The PBE0 model. J. Chem. Phys. 1999;110:6158–70.
[27] Francl MM, Pietro WJ, Hehre WJ, Binkley JS, Gordon MS, DeFrees DJ, Pople JA. Self–consistent molecular orbital methods. xxiii. a polarization–type basis set for second–row elements. J. Chem. Phys. 1982;77:3654–65.
[28] Ufimtsev IS, Martinez TJ. Quantum chemistry on graphical processing units. 3. analytical energy gradients, geometry optimization, and first principles molecular dynamics. J. Chem. Theory Comput. 2009;5(10):2619–28.
[29] Cruz JC, Hernández-Esparza R, Vázquez-Mayagoitia A, Vargas R, Garza J. Implementation of the molecular electrostatic potential over graphics processing units. J. Chem. Inf. Model. 2019;59:3120–7.
[30] Johnson ER, Keinan S, Mori-Sánchez P, Contreras-García J, Cohen AJ, Yang W. Revealing noncovalent interactions. J. Am. Chem. Soc. 2010;132(18):6498–506.
[31] Hernández-Esparza R, Mejía-Chica SM, Zapata-Escobar AD, Guevara-García A, Martínez-Melchor A, Hernández-Pérez JM, Vargas R, Garza J. Grid-based algorithm to search critical points, in the electron density, accelerated by graphics processing units. J. Comput. Chem. 2014;35(31):2272–8.
[32] Hernández-Esparza R, Vázquez-Mayagoitia A, Soriano-Agueda LA, Vargas R, Garza J. GPUs as boosters to analyze scalar and vector fields in quantum chemistry. Int. J. Quantum Chem. 2019;119:e25671.
[33] Vargas R, Garza J, Dixon D, Hay B. How strong is the C-alpha-H center dot center dot center dot O=C hydrogen bond? J. Am. Chem. Soc. 2000;122:4750–5.
[34] Yang L, Hubbard TA, Cockroft SL. Can non-polar hydrogen atoms accept hydrogen bonds? Chem. Commun. 2014;50:5212–4.
[35] Espinosa E, Molins E, Lecomte C. Hydrogen bond strengths revealed by topological analyses of experimentally observed electron densities. Chem. Phys. Lett. 1998;285:170–3.